Physica Scripta

Tunable nonlinear absorption and optical limiting behavior of $NaBi(Mo_xW_{1-x}O_4)_2$ single crystals with ratio of Molybdenum/Tungsten

Physica Scripta

PAPER

Tunable nonlinear absorption and optical limiting behavior of $NaBi(Mo_xW_{1-x}O_4)_2$ single crystals with ratio of Molybdenum/Tungsten

Yasemin Pepe[1], **Elif Akhuseyin Yildiz**[1], **Mehmet Isik**[2], **Ahmet Karatay**[1,*], **Nizami Gasanly**[3] and **Ayhan Elmali**[1]

[1] Department of Engineering Physics, Faculty of Engineering, Ankara University, 06100 Ankara, Turkey
[2] Department of Electrical and Electronics Engineering, Atilim University, 06836 Ankara, Turkey
[3] Department of Physics, Science and Art Faculty, Middle East Technical University, 06800 Ankara, Turkey
[*] Author to whom any correspondence should be addressed.

E-mail: akaratay@eng.ankara.edu.tr

Keywords: $NaBi(MoxW_{1-x}O_4)_2$ single crystals, open aperture Z-scan technique, nonlinear absorption, defect states, optical limiting

OPEN ACCESS

RECEIVED
1 March 2023

REVISED
11 May 2023

ACCEPTED FOR PUBLICATION
1 June 2023

PUBLISHED
14 June 2023

Abstract

The compositional effect of Mo/W ratio on linear, nonlinear absorption and optical limiting behavior of the $NaBi(Mo_xW_{1-x}O_4)_2$ single crystals grown by Czochralski technique was investigated. X-ray diffraction patterns of the studied crystals presented well-defined peaks associated with the tetragonal crystalline structure. The nonlinear absorption performance and optical limiting threshold were determined using an open-aperture Z-scan technique. A theoretical model including one photon absorption (OPA), two photon absorption (TPA) and free carrier absorption was used to determine the nonlinear absorption parameters. All of the results showed that defect states, which strongly affect nonlinear absorption (NA) and optical limiting behaviors, can be tuned with the Mo/W ratio, enabling $NaBi(Mo_xW_{1-x}O_4)_2$ single crystals to be used in desired optoelectronic applications. Linear optical absorption analysis revealed that bandgap energy and defect states can be tuned by changing the Mo/W ratio in the crystal structure. The obtained results showed that all the studied crystals had NA behavior and the nonlinear absorption coefficient decreased with increasing Mo/W ratio. Sequential TPA is the main NA mechanism for these crystals due to the fact that the incident light energy is lower than the bandgap energies and the existence of the real intermediate state around 2.32 eV.

1. Introduction

Double tungstates and molybdates formulated as $AB(YO_4)_2$ (A: monovalent cation; Li^+, Na^+ or K^+, B: trivalent one; Ln^{3+}, Y^{3+}, or Bi^{3+}, Y: Mo^{6+} or W^{6+}) have been a significant research interest thanks to their structural and optical features [1, 2]. These compounds crystallize in two phases belonging to the monoclinic and tetragonal structures [1].The high refractive index, nonlinear optical characteristics, luminescence properties, wide transmission range and large optical bandwidths make these compounds potential candidates in laser, light emitting diode, optical amplifier, and nonlinear optical device applications [3–5]. $NaBi(WO_4)_2$ and $NaBi(MoO_4)_2$ are two members of this group and the device applications of these compounds are increasing in recent years. Device application studies indicated that $NaBi(MoO_4)_2$ and $NaBi(WO_4)_2$ may be used in light emitting diodes, scintillators, temperature sensors, gas sensing devices [6–11]. Both compounds crystallize in tetragonal structure with reported lattice parameters of $a = b = 5.272$ Å, $c = 11.577$ Å for NaBi(MoO4)2 and $a = b = 5.265$ Å, $c = 11.429$ Å for NaBi(WO4)2 [12–14]. In the crystal structure, each Mo and W element is attached to four O-atoms and thanks to these bonds, MoO_4 and WO_4 tetrahedron structure are formed. Random distribution of Na^+ and Bi^{3+} atoms in the crystal structure caused these compounds to have a disordered structure. $NaBi(WO_4)_2$ and $NaBi(MoO_4)_2$ compounds can be synthesized/grown in single crystal,

thin film and nano structures. Although this situation causes changes in the band energies of the compounds, the bandgap energies of $NaBi(MoO_4)_2$ and $NaBi(WO_4)_2$ are generally reported to be around 2.90 and 3.50 eV, respectively [14–17].

$NaBi(Mo_xW_{1-x}O_4)_2$ compounds are formed as a result of replacing Mo element with W element. The most important advantage of obtaining such compounds is that the structural and optical properties can be adjusted depending on the composition. The tuning behavior of the optical characteristics supplies a noteworthy advantage especially in optoelectronic applications. For example, the photoluminescence study on $GaS_{1-x}Se_x$ nanobelts showed that the materials give emissions that vary with the composition in the range of 490–620 nm (2.0–2.5 eV) [18]. It is possible to design a device emitting specific light within this region by adjusting the composition. The studies on $Zn_xMg_{1-x}O$ indicated that crystal structure and emission characteristics change depending on the composition [19]. It was reported in [19] that Mg-rich compounds may be used to design optoelectronic devices operating at deep UV range. There are limited studies on $NaBi(Mo_xW_{1-x}O_4)_2$ compounds in the literature. In our recent study, the structural and optical properties of $NaBi(Mo_{0.5}W_{0.5}O_4)_2$ single crystal were reported [13]. The direct bandgap and Urbach energies of the crystal were reported as 3.18 and 0.17 eV, respectively [13]. A recent paper reported the microwave dielectric properties of compounds corresponding to compositions of $x = 0.0$, 0.5 and 1.0 [20]. The reported characteristics indicated that $(Na_{0.5}Bi_{0.5})(Mo_{1-x}W_x)O_4$ ceramics have significant potential to be utilized in low temperature co-fired ceramic area. Considering the device application effectiveness of the $NaBi(Mo_xW_{1-x}O_4)_2$ compounds, the present paper aimed at investigating NA characteristics of the single crystals of compositions $x = 0$, 0.5 and 0.75. NA and optical limiting characteristics of these compounds were revealed for the first time with this study. For this purpose, open aperture (OA) Z-scan measurements were accomplished at 532 nm irradiation wavelength by increasing the input densities to reveal NA behavior of the $NaBi(Mo_xW_{1-x}O_4)_2$ single crystals. Optical limiting characteristics were also investigated. The dependence of the revealed optical parameters on Mo/W ratio was discussed throughout the paper.

2. Experimental section

2.1. Growth of $NaBi(Mo_xW_{1-x}O_4)_2$ single crystals

$NaBi(Mo_xW_{1-x}O_4)_2$ single crystals for compositions of $x = 0$, 0.5 and 0.75 were grown by Czochralski method [13, 21]. Bi_2O_3, MoO_3, WO_3 and Na_2CO_3 starting compounds were used in the required ratios for each crystal. The starting compounds used in stoichiometric ratios were mixed and then pelleted. The pellets were heated at 700 °C–800 °C for 20–24 h to obtain a single phase. Throughout the growing process, 2 mm h^{-1} pulling rate and 15 rpm rotation rate was applied. After the end of the crystal growth process, small rectangular prism-shaped pieces were cut from the large ingot and these pieces were polished. $NaBi(Mo_xW_{1-x}O_4)_2$ single crystals for x = 0, 0.5 and 0.75 were represented as crystals 1, 2 and 3 in this report.

2.2. Characterization methods

X-ray diffraction (XRD) experiments are used to analysis of structural characterization of the grown crystals. Rigaku miniflex model diffractometer emitting CuK_α radiation at wavelength of 0.154049 nm from 20 to 50° with a speed of 0.02°/s was used for XRD measurements. The thicknesses of the single crystals were measured at around 0.4 cm. UV-1800 model Shimadzu UV–vis spectrophotometer was used to reveal the linear optical behavior of the $NaBi(Mo_xW_{1-x}O_4)_2$ (at x = 0, 0.5 and 0.75) single crystals. OA Z-scan experiments with Q-switched Nd:YAG (Quantel Birillant) laser (10 Hz repetition rate, 4 ns pulse duration) at 532 nm excitation wavelength were carried out to determine nonlinear optical behavior of the crystals. The beam waist radius (ω_0) at the focus was used as 22 μm, Rayleigh length were calculated to be 2.85 mm for 532 nm. The OA experiments were performed at 0.8, 2.7 and 4 μJ input energies and at 13.23, 44.10 and 66.16 MW cm^{-2} the input intensities.

3. Results and discussions

3.1. Materials characterizations

Figure 1 depicts the XRD patterns of $NaBi(Mo_xW_{1-x}O_4)_2$ crystals. XRD patterns show sharp peaks at 31.30° and 64.95° for crystal 1, 34.60° and 70.00° for crystal 2, 35.20° and 70.90° for crystal 3. The presence of these peaks shows that grown compounds were successfully obtained in single crystal form. The peaks seen in the XRD patterns of crystals 1 and 2 are in good accordance with the literature's previously published peaks [13]. Considering the [20], the observed peaks are related to tetragonal crystalline structure of the studied crystals and figure 1 shows the corresponding Miller indices on the peaks. When the positions of the peaks observed for each crystal in the figure were compared, it was seen that the angle position of the peaks seen at high degrees corresponded to almost twice the angle position of the peaks seen at low degrees. This shows that the planes of

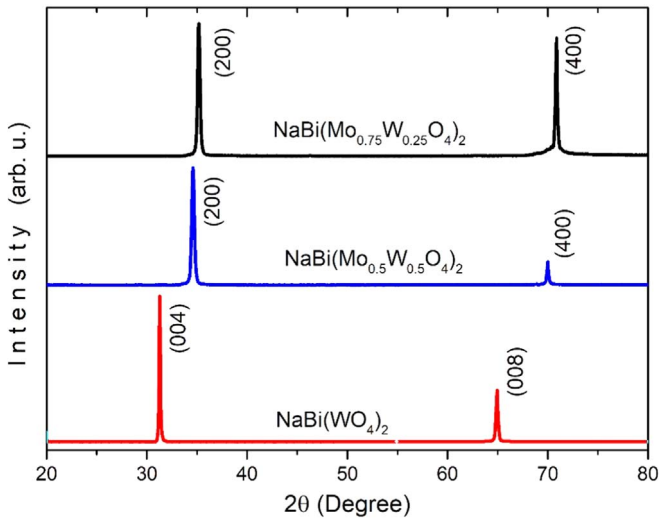

Figure 1. XRD patterns of single crystals 1, 2 and 3.

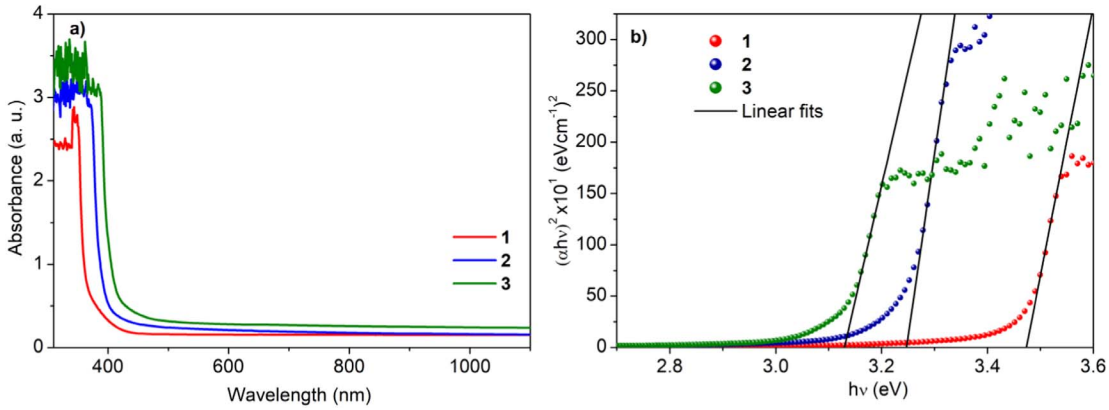

Figure 2. (a) Linear absorption spectra and (b) $(\alpha h\nu)^2$ versus $h\nu$ graphs (Tauc plots) of crystals 1, 2 and 3.

the respective peaks are parallel to each other. For example, the (200) plane of the peak at 35.20° observed for crystal 3 is parallel to the (400) plane of the peak at 70.90°. This can be interpreted as the orientation of crystal surfaces in a single plane. The values of particle sizes (D) were were found to be 61.02, 29.92 and 44.43 nm for 1, 2 and 3 crystals, respectively, which were calculated using the Scherrer's equation ($D = 0.94\lambda/\beta\cos\theta$) [22]. Herein, θ is the Bragg angle, β is the FWHM and λ refers to the wavelength of the x-ray.

3.2. Linear absorption analysis

Figure 2(a) indicates linear absorption behavior of crystals 1, 2 and 3. The Mo/W ratios are 0, 1 and 3 for crystal 1, 2 and 3, respectively. As can be seen from this figure, the increased Mo/W ratio resulted in increased absorption with slightly shifted absorption band edge towards the longer wavelength. The energy of forbidden bandgap is obtained by the following expression [23]

$$\alpha h\nu = A(h\nu - E_g)^n \tag{1}$$

where $n = 1/2$ and $n = 2$ for direct and indirect transitions taking place between valence and conduction bands, E_g is forbidden bandgap energy, α is absorption coefficient, A is a constant and $h\nu$ is photon energy. Due to the direct transition of the crystals 1, 2 and 3, $(\alpha h\nu)^2$ versus $h\nu$ graphs (Tauc plot) presented in figure 2(b) give the E_g values of the studied single crystals. The E_g values are found as 3.47, 3.24 and 3.13 eV for crystals 1, 2 and 3. The reported bandgap energies of the $NaBi(MoO_4)_2$ and $NaBi(WO_4)_2$ crystals are around 2.90 and 3.50 eV, respectively [14, 15]. It is clearly seen that increasing Mo/W ratio in the crystal led to decreasing bandgap energy. This also means that the E_g value of $NaBi(Mo_xW_{1-x}O_4)_2$ single crystals can be adjusted for desired optoelectronic

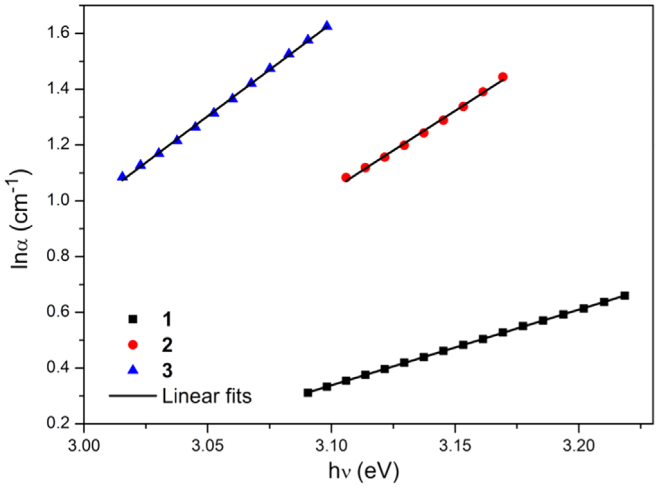

Figure 3. $ln\alpha$ versus $h\nu$ plot of crystals 1, 2 and 3.

applications by varying the Mo/W ratio. The tuning characteristics of the bandgap energy of NaBi(MoxW1-xO4)2 compounds provide a remarkable advantage for optoelectronic applications.

Nonlinear optical behavior and nonlinear absorption mechanisms are strongly associated with the defects in the structure as well as bandgap energy of the materials [24–28]. The tail width of absorption band edge, known as the Urbach tail, is used to reveal the defects just below the conduction band using the following expression [29]

$$\alpha = \alpha_0 \exp\left(h\nu/E_U\right) \tag{2}$$

where α_0 is a constant, E_U is the Urbach energy and α is the linear absorption coefficient. The inverse slope of the linear region of the $ln\alpha$ with respect to $h\nu$ graphs presented in figure 3 provides the E_U values of the samples. The values of $E_U$are calculated as 0.37, 0.17 and 0.15 eV for crystals 1, 2 and 3, respectively. Decreasing E_U value with increase of the Mo/W ratio is the evidence of the decreasing defects in the structure [30, 31].

3.3. Nonlinear absorption and optical limiting analysis

OA Z-scan measurements are conducted at 532 nm irradiation wavelength under several input densities to bring out the NA properties of 1, 2 and 3 single crystals. The data of Z-scan are analyzed using a theoretical model that takes into account the contribution of one-photon absorption (OPA), two-photon absorption (TPA) and free carrier absorption (FCA) to NA.

$$\frac{dI}{dz'} = \frac{\alpha I}{1 + I/I_{SAT}} - \frac{\beta_{eff} I^2}{1 + I^2/I_{SAT}^2} \tag{3}$$

In this model, the first term represents the OPA and its saturation, the second term represents TPA, FCA and their saturations. In equation (3), I_{SAT} is the saturation intensity threshold and β_{eff} is the effective NA coefficient and it is given as below.

$$\beta_{eff} = \beta + (\sigma_0 \alpha \tau_0/\hbar\omega) \tag{4}$$

The fitting details are given in [32]. The curves of OA Z-scan of the crystals 1, 2 and 3 at various input intensities are shown in figure 4. When the input intensity increased, the normalized transmittance for crystal 1 decreased. Contrarily, for crystals 2 and 3, the normalized transmittance increased as the input intensity increase. Due to lower energy of the incident light (2.32 eV) than that of the bandgap energies of the single crystals, the main NA mechanism is TPA for studied crystals. On the other hand, the presence of intermediate states allows the differentiation of two types of TPA: (i) genuine TPA, which involves simultaneous absorption of two photons through a virtual state, and (ii) sequential TPA also known as OPA + ESA (excited state absorption) is sequential absorption of two photons [33]. Intermediate states created by defects lead to enhanced depletion of the ground state population, resulting in increased ESA. Genuine TPA is common when the NA coefficient is independent of the input density. However, when the NA coefficient changes (increases/decreases) with increasing input density, the ESA process will become dominant. Z-scan cannot reveal the nature of TPA, therefore, intensity-dependent NA assessment is necessary to ascertain the true mechanism behind TPA. Therefore, the graph of variation β_{eff} by input density is presented in figure 5. According to this figure, the studied crystals have real intermediate states in the energy region of 2.32 eV. NA decreased with increasing input

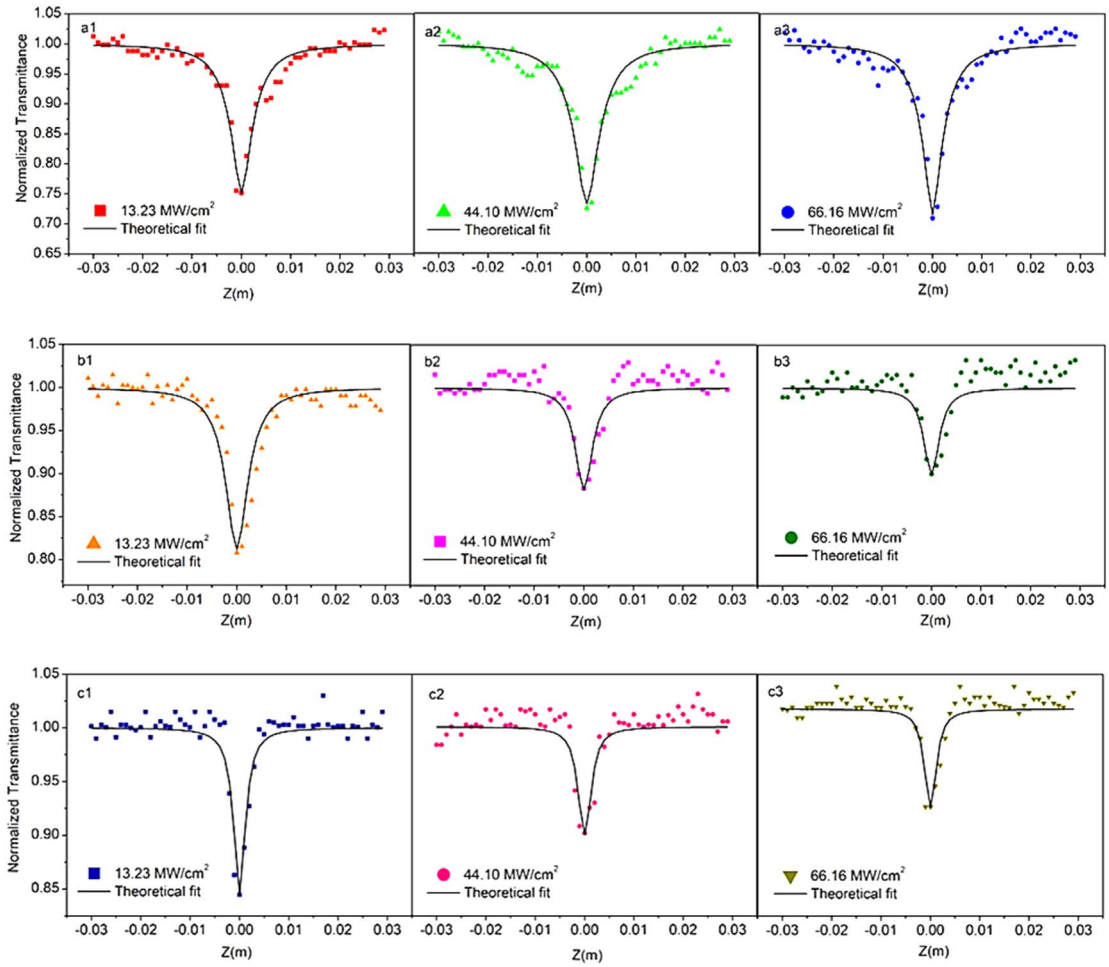

Figure 4. OA Z-scan curves of crystals 1 (a1)–(a3), 2 (b1)–(b3) and 3 (c1)–(c3) at 532 nm under various input intensities.

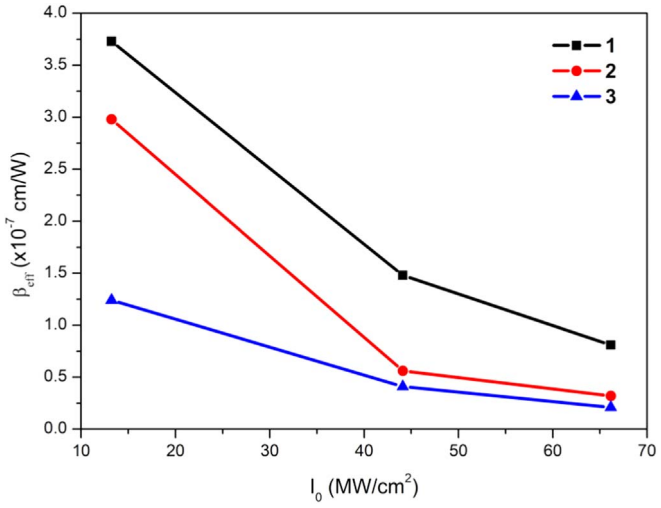

Figure 5. Variation of β_{eff} with respect to input intensities.

densities due to defect states corresponding to the energy region of 2.32 eV being filled by OPA. Therefore, the main NA mechanism is sequential TPA for these crystals.

The normalized transmittances of single crystals at 66.16 MW cm^{-2} are presented in figure 6. The obtained β_{eff} are found to be 3.73 $\times 10^{-7}$, 2.98 $\times 10^{-7}$ and 1.24 $\times 10^{-7}$ cm W^{-1}, and the I_{SAT} values are obtained as 6.63 $\times 10^{9}$, 3.86 $\times 10^{9}$ and 1.80 $\times 10^{9}$ W/cm^2 for crystals 1, 2 and 3, respectively. Decreased β_{eff} is obtained for

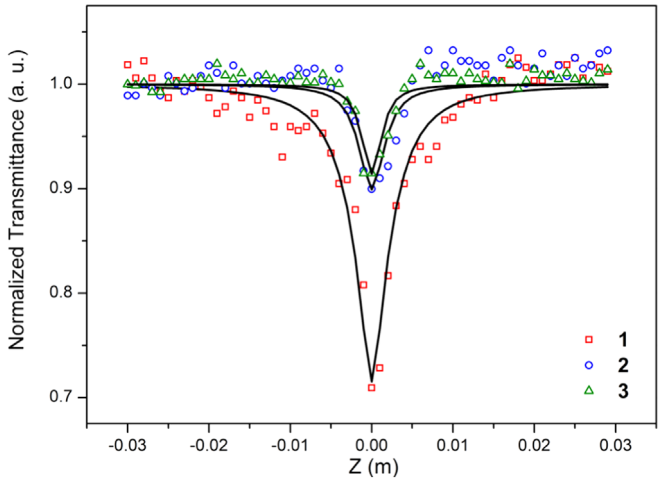

Figure 6. OA Z-scan curves of the crystals 1, 2, and 3 at 66.16 MW cm^{-2} input intensity.

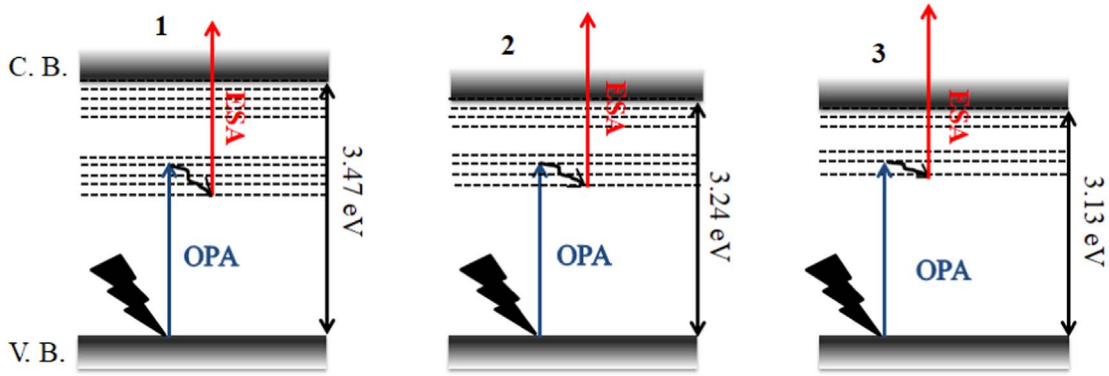

Figure 7. A schematic for the proposed NA mechanisms for the crystals 1, 2, and 3.

increasing Mo/W ratio and a similar trend is observed for I_{SAT} values. The schematic of the proposed NA mechanisms for these single crystals were given in figure 7. All of the single crystals have the same NA mechanism (sequential TPA). On the other hand, their defect states density created differences on the power of NA behaviors. Their defect states density were displayed in figure 7 as dash line. S.G. Singh et all [34] reported five defect centers around 3.1, 2.8, 2.6, 2.0 and 1.7 eV for $NaBi(WO_4)_2$ which is represented as crystal 1 in this study. According to figure 5, it was also said that the crystal 2 and 3 have defect states at around 2.32 eV energy region inside the band gap. The observing increasing normalized transmittance (figure 4) can be attributed to lower defect states of crystal 2 and 3 at around 2.32 eV as compared to crystal 1. These lower density of the defect states were filled by OPA and the saturable absorption effect on the NA led to weaker NA behavior as compared to crystal 1. All of the results indicated that the crystal 1 has higher β_{eff} among other single crystals due to its higher defect states. We reported the effect of the defect states on the NA behavior of the single crystals in our previous studies [35–37].

An excellent optical limiter for efficient limiting at intense laser beam is composed of FCA, TPA, ESA, nonlinear refraction and nonlinear scattering [38]. As the optical limiters are essential for protecting optically sensitive equipment from hazardous laser light, their development takes great attention [39–41]. An efficient optical limiter limits the transmitted light intensity over its optical limiting threshold and holds it constant, and in this way it protects the sensitive devices. It is well known that a lower optical limiting threshold causes higher optical limiting response. Figure 8 demonstrates the normalized transmission curves as a function of fluence. The distance dependent fluence relation is given by the following equation [42],

$$I(z) = \frac{E}{\pi\omega^2(z)t} \tag{5}$$

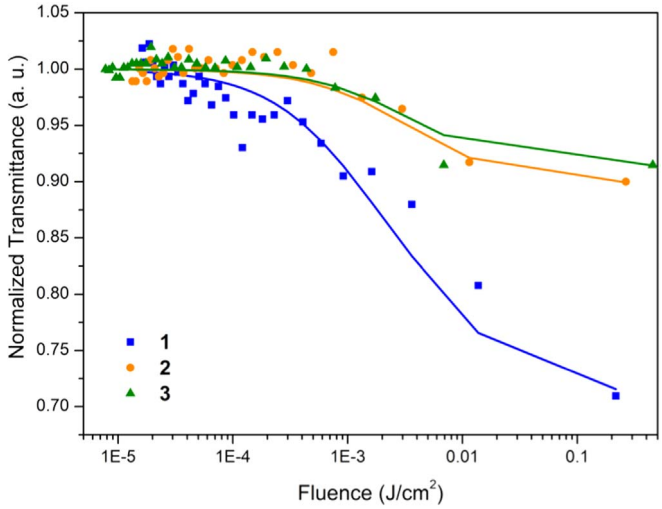

Figure 8. Optical limiting curves of crystals 1, 2 and 3 at 66.16 MW cm^{-2} input intensity.

where E is the input energy per pulse and t is the pulse duration, $\omega(z)$ is the beam waist as a function of distance and it can be determined by following the relation for Gaussian beam waist,

$$\omega^2(z) = \omega_0^2\left(1 + \frac{z^2}{z_R^2}\right) \tag{6}$$

$$z_R = \frac{\pi\omega_0^2}{\lambda} \tag{7}$$

where z_R is the Rayleigh distance, λ is the wavelength of the input light, and ω_0 is the beam waist at focus. Optical limiting thresholds are found to be 5.19×10^{-2}, 3.39×10^{-1} and 4.38×10^{-1} mJ/cm^2 for crystals 1, 2 and 3, respectively. It is clearly seen that stronger NA behavior triggers higher optical limiting behavior. Among other crystals, crystal 1 showed stronger optical limiting behavior.

4. Conclusions

NA and optical limiting characteristics of the $NaBi(Mo_xW_{1-x}O_4)_2$ single crystals for x = 0, 0.5 and 0.75 grown by Czochralski technique were reported in this study. XRD patterns of the crystals presented one peak associated with tetragonal crystalline structure. Linear optical absorption analysis revealed that the bandgap energy decreased from 3.47 to 3.13 eV with increasing concentration of the Mo with respect to W atom in the crystal structure. In addition, the Urbach energy decreased from 0.37 to 0.15 eV with increasing ratio of Mo/W. To investigate the NA behaviors, the OA Z-scan experiments were performed at 532 nm considering OPA, TPA and FCA absorption contributions to NA. Obtained results indicated that all of the studied crystals possess NA behavior. Due to the lower energy of the incident light than the bandgap energy, and the presence of the real intermediate state corresponding to 2.32 eV, the sequential TPA is the dominant NA mechanisms for these crystals. Obtained β_{eff} value decreased from 3.73×10^{-7} to 1.24×10^{-7} cm W^{-1}, and I_{SAT} value decreased from 6.63×10^9 to 1.80×10^9 W cm^{-2} with increasing ratio of Mo/W in the crystal structure. Stronger NA behavior was observed for $NaBi(WO_4)_2$ single crystal possessing higher Urbach energy among other crystals. Lower optical limiting threshold was obtained to be 5.19×10^{-2} mJ/cm^2 for $NaBi(WO_4)_2$ single crystal which is includes lower Mo/W ratio. All of the results revealed that the bandgap energy can be tunable with the adjustment of the Mo/W ratio to use of the $NaBi(Mo_xW_{1-x}O_4)_2$ single crystals for the optoelectronic application in wide spectral range.

Data availability statement

All data that support the findings of this study are included within the article (and any supplementary files).

ORCID iDs

Yasemin Pepe https://orcid.org/0000-0002-5384-2039
Elif Akhuseyin Yildiz https://orcid.org/0000-0001-6485-4660
Ahmet Karatay https://orcid.org/0000-0001-9373-801X

References

[1] Zharikov E V, Zaldo C and Diaz F 2009 Double tungstate and molybdate crystals for laser and nonlinear optical applications *MRS Bull.* **34** 271–6
[2] Laguna M, Nunez N O, Becerro A I, Lozano G, Moros M, de la Fuente J M, Corral A, Balcerzyk M and Ocana M 2019 Synthesis, functionalization and properties of uniform europium-doped sodium lanthanum tungstate and molybdate (NaLa(XO4)(2), X = Mo, W) probes for luminescent and x-ray computed tomography bioimaging *J. Colloid Interf. Sci.* **554** 520–30
[3] Han W J, Dong L, Zhang Y X, Xu H H and Liu J H 2023 Comparative study on passive Q-switching laser properties of Yb:CaWO4 and Yb:NaY(WO4)(2) crystals *Opt. Mater.* **137** 113571
[4] Tan S Y, Wang X S, Zhao Y, Li Y X and Yao X 2023 Strong luminescence intensity and high temperature sensitivity of Er3+-doped KYb (MoO4)2 phosphors optimized by codoping trivalent ions *J. Lumin.* **257** 119747
[5] Mu B Q, Huang J R, Song R S, Dong Y Q and Qi B 2023 Optical analysis of Dy3+/Sm3+co-doped NaY(MoO4)2 phosphors for warm white LED *J. Alloy Compd.* **945** 168916
[6] Xie J H, Cheng L Q, Tang H, Yu X F, Wang Z X, Mi X Y, Liu Q S and Zhang X Y 2022 Synthesis and photoluminescence properties of NUV-excited NaBi(MoO4)(2): Sm3+ phosphors for white light emitting diodes *Opt. Laser Technol.* **147** 107659
[7] Xie J H, Cheng L Q, Tang H, Yu X F, Wang Z X, Mi X Y, Liu Q S and Zhang X Y 2021 A new single-phase NaBi(WO4)(2):Dy3+, Eu3+ phosphor with excellent thermal stability for NUV-excited warm white LEDs *J. Alloy Compd.* **882** 160589
[8] Xie J H, Cheng L Q, Tang H, Yu X F, Wang Y T, Wang C B, Mi X Y, Liu Q S and Zhang X Y 2020 Synthesis and photoluminescence properties of NaBi(WO4)(2):Eu3+ red-emitting phosphor for NUV-based WLEDs *J. Lumin.* **219** 116841
[9] Tyagi M, Singh S G, Sen S, Singh A K and Gadkari S C 2012 Photoluminescence and photoconductivity studies on NaBi(WO4)(2) single crystals: a promising Cherenkov radiator *J. Lumin.* **132** 41–5
[10] Ren X T, Gao J, Shi H N, Zhao S L, Huang L H and Xu S Q 2021 A flexible and portable all-fiber temperature sensor based on the upconversion luminescence of octahedral NaBi(WO4)(2):Er3+/Yb3+ phosphors *Dalton T* **50** 917–25
[11] Qian H Y, Zhang T Q, Jiang X L, Wang H H, Yang W L and Li C 2022 Visible photon avalanche up-conversion of Yb3+ and Ho3+ doped NaBi(WO4)(2) phosphors under excitation at 980 nm *J. Mater Sci.-Mater. El* **33** 22718–27
[12] Gan Y, Liu W, Zhang W T, Li W J, Huang Y and Qiu K H 2019 Effects of Gd3+ codoping on the enhancement of the luminescent properties of a NaBi(MoO4)(2):Eu3+ red-emitting phosphors *J. Alloy Compd.* **784** 1003–10
[13] Isik M, Guler I and Gasanly N M 2023 Growth and characterization of NaBi(Mo0.5W0.5O4)(2) single crystal: a promising material for optoelectronic applications *Mat. Sci. Semicon. Proc.* **156** 107257
[14] Isik M, Gasanly N M, Darvishov N H and Bagiev V E 2022 Temperature dependent bandgap in NaBi(WO4)(2) single crystals *Optik* **258** 168811
[15] Liu J X, Wei R J, Hu J C, Li L Z and Li J L 2013 Novel Bi2O3/NaBi(MoO4)(2) heterojunction with enhanced photocatalytic activity under visible light irradiation *J. Alloy Compd.* **580** 475–80
[16] Shi H F, Li Z S, Ye J H and Zou Z G 2010 2-propanol photodegradation over molybdates: effects of chemical compositions and electronic structures *J. Phys. D: Appl. Phys.* **43** 085402
[17] Tyagi M, Singh S G, Prasad S R, Auluck S and Singh D J 2010 A study of electronic and optical properties of NaBi(WO4)(2): A disordered double tungstate crystal *Physica B* **405** 3267–71
[18] Jung C S *et al* 2016 Photoluminescence and Photocurrents of $GaS_{1-x}Se_x$ Nanobelts *Chem. Mater.* **28** 5811–20
[19] Vanjaria J V, Azhar E A and Yu H B 2016 Broad range tuning of structural and optical properties of ZnxMg1-xO nanostructures grown by vapor transport method *J. Phys. D: Appl. Phys.* **49** 465103
[20] Pang L X, Zhou D, Qi Z M and Yue Z X 2017 Influence of W substitution on crystal structure, phase evolution and microwave dielectric properties of (Na0.5Bi0.5)MoO4 ceramics with low sintering temperature *Sci. Rep.* **7** 3201
[21] Mendez-Blas A, Rico M, Volkov V, Zaldo C and Cascales C 2007 Crystal field analysis and emission cross sections of Ho3+ in the locally disordered single-crystal laser hosts M+Bi(XO4)(2) (M+ = Li, Na; X = W, Mo) *Phys. Rev.* **75** 174208 B
[22] Holzwarth U and Gibson N 2011 The Scherrer equation versus the 'Debye–Scherrer equation' *Nat. Nanotechnol.* **6** 534–534
[23] Pankove J I 1972 Optical processes in semiconductors *J. Electrochem. Soc.* **119** 156Ca
[24] Guichaoua D, Syvorotka I, Solskii I, Syvorotka N, Waszkowska K, Andrushchak A and Sahraoui B 2021 Specific complex-oxide crystals with strong nonlinear absorption and nonlinear refraction as promising optical materials *Opt. Mater.* **121** 111493
[25] Unlu B A, Karatay A, Yildiz E A, Yola M L, Yuksek M, Atar N and Elmali A 2021 Defect assisted optical limiting performance of hexagonal boron nitride nanosheets in aqueous suspension and PMMA nanocomposite films *Opt. Mater.* **121** 111630
[26] Pepe Y, Akkoyun S, Bozkurt B, Karatay A, Ates A and Elmali A 2022 One-photon absorption enhanced nonlinear absorption and optical limiting of the electrospun polyvinylpyrrolidone via excitation energy and incorporation of polypyrrole particles *J. Mater. Sci.* **57** 21265–21275
[27] Karatay A, Yuksek M, Ertap H, Mak A K, Karabulut M and Elmali A 2016 Influence of boron concentration on nonlinear absorption and ultrafast dynamics in GaSe crystals *Opt. Mater.* **60** 74–80
[28] Karatay A, Aksoy C, Yaglioglu H G, Elmali A, Kurum U, Ates A and Gasanly N 2011 The nonlinear and saturable absorption characteristics of Ga0.90In0.10Se and Ga0.85In0.15Se semiconductor crystals and their amorphous thin films *J. Optics-Uk* **13** 075203
[29] Urbach F 1953 The long-wavelength edge of photographic sensitivity and of the electronic absorption of solids *Phys. Rev.* **92** 1324–1324
[30] Pepe Y, Tutel Y, Yildiz E A, Karatay A, Unalan H E and Elmali A 2021 Thermally induced phase transition and defect-assisted nonlinear absorption and optical limiting in nanorod morphology V_2O_5 thin films *Adv. Eng. Mater.* **23** 2100468
[31] Pepe Y, Akkoyun S, Bozkurt B, Karatay A, Ates A and Elmali A 2023 Defect-assisted wavelength dependence of one photon and multiphoton absorptions in a composite nanofiber of polyvinylpyrrolidone and hexagonal boron nitride *J. Mater. Chem. C* **11** 2756–63
[32] Yuksek M, Kurum U, Yaglioglu H G, Elmali A and Ates A 2010 Nonlinear and saturable absorption characteristics of amorphous InSe thin films *J. Appl. Phys.* **107** 033115

[33] Zheng X Q, Feng M and Zhan H B 2013 Giant optical limiting effect in Ormosil gel glasses doped with graphene oxide materials *J. Mater. Chem. C* **1** 6759–66
[34] Singh S G, Tyagi M, Desai D G, Singh A K and Gadkari S C 2010 Radiation damage studies on NaBi(WO4)(2) single crystals through oxygen related defects *Nucl. Instrum. Meth. A* **621** 111–5
[35] Pepe Y, Isik M, Karatay A, Gasanly N and Elmali A 2023 Wavelength dependence of the nonlinear absorption performance and optical limiting in Bi12TiO20 single crystal *J. Lumin.* **253** 119494
[36] Pepe Y, Isik M, Karatay A, Gasanly N and Elmali A 2022 Nonlinear optical absorption characteristics of PbMoO4 single crystal for optical limiter applications *Opt. Mater.* **133** 112963
[37] Pepe Y, Isik M, Karatay A, Yildiz E A, Gasanly N and Elmali A 2022 The role of defects on the transition from saturable absorption to nonlinear absorption of Bi12GeO20 single crystal under increasing laser excitation *J. Lumin.* **251** 119170
[38] Saravanan M and Girisun T C S 2015 Nonlinear optical absorption and optical limiting properties of cadmium ferrite *Mater. Chem. Phys.* **160** 413–9
[39] Savelyev M S, Gerasimenko A Y, Podgaetskii V M, Tereshchenko S A, Selishchev S V and Tolbin A Y 2019 Conjugates of thermally stable phthalocyanine J-type dimers with single-walled carbon nanotubes for enhanced optical limiting applications *Opt. Laser Technol.* **117** 272–9
[40] Abdullah A, Yudono A, Adisasmita S A and Akil A 2019 Determination of the location intercity bus transit in makassar city using expert system model and gis *Journal of Theoretical and Applied Information Technology* **97** http://jatit.org/volumes/Vol97No2/12Vol97No2.pdf
[41] Praveen P A, Prabhakaran S P, Babu R R, Sethuraman K and Ramamurthi K 2015 Low power optical limiting studies on nanocrystalline benzimidazole thin films prepared by modified liquid phase growth technique *B Mater. Sci.* **38** 645–51
[42] Sreeja V G, Hajara P, Reshmi R and Anila E I 2021 Effects of reduced graphene oxide on nonlinear absorption and optical limiting properties of spin coated aluminium doped zinc oxide thin films *Thin Solid Films* **722** 138580